Processes of intraseasonal snow cover variations over the eastern China during boreal winter

Lei Song[1], Renguang Wu[2,1,3*] and Jialei Zhu[4]

[1]*Center for Monsoon System Research, Institute of Atmospheric Physics, Chinese Academy of Sciences, Beijing, China*

[2]*School of Earth Sciences, Zhejiang University, Hangzhou, China*

[3]*State Key Laboratory of Numerical Modeling for Atmospheric Sciences and Geophysical Fluid Dynamics, Institute of Atmospheric Physics, Chinese Academy of Sciences, Beijing, China*

[4]*Department of Climate and Space Sciences and Engineering, University of Michigan, Ann Arbor, USA*

Atmospheric Science Letters

Submitted February 23, 2019

Revised March 29, 2019

**Corresponding author address:*

Renguang Wu

Institute of Atmospheric Physics, Chinese Academy of Sciences

Building 40, Huayanli, Beichen West Road, Chaoyang, Beijing 100029, China

E-mail: renguang@mail.iap.ac.cn

Key words: Intraseasonal snow cover variation, the eastern China, AO, moisture fluxes

Abstract

This study reveals that the dominant time scale of intraseasonal snow cover variation over the eastern China is within 30 days by using the latest satellite snow cover data from the MODIS/Terra product. The leading EOF mode of 10-30-day snow cover variation during boreal winter from 2004 to 2018 over the eastern China has two centers: northwest part of the eastern China and north of the Yangtze River. Composite analysis based on 25 snow events identified from normalized PC1 indicates that the southeastward intrusion of surface anticyclonic anomalies and accompanying low temperature anomalies provide the temperature condition for snow events. Negative AO induces mid-latitude wave train and leads to the development of surface anticyclonic anomalies and upper-level cyclonic anomalies over East Asia. The cyclonic anomalies induce ascending motion and anomalous convergence of water vapor fluxes over the eastern China, which supplies moisture for snowfall.

1. Introduction

In January 2008, a strong ice storm with snowfall hit the eastern China (Zhou et al. 2011), one of the most populated regions in East Asia. Unlike northeastern China and the Tibetan Plateau, the eastern China (20-40°N, 105-120°E) is not usually covered by snow during boreal winter (Wen et al. 2009). So, the snowfall over this region caused tremendous economic losses (Wen et al. 2009; Zhou et al. 2009). The study by Sun et al. (2010) and Zhou et al. (2018) suggested that the snowfall events over the eastern China tend to be isolated from other regions of China.

The occurrence of snowfall events over the eastern China on synoptic scale has been discussed by previous studies (Wen et al. 2009; Zhou et al. 2009; Gao 2009; Zhou et al. 2010). Previous studies have also documented interannual to interdecadal snow variation over the eastern China (Sun et al. 2010; Zhou et al. 2017, 2018). There are relatively few studies on snow variations on intraseasonal time scales. The investigation of the intraseasonal variation of snow and the factors and processes can help to improve the predictive skill of snowfall.

The occurrence of snowfall requires both low temperature and large amount of moisture (Sun and Wang 2013; Zhou et al. 2018). Previous studies have indicated that the occurrence of snowfall events over the eastern China is related to the strong western Pacific subtropical high and the Indian-Burma trough that help to transfer

moisture toward the eastern China (Zhou et al. 2009; Li et al. 2017), the variation of the subtropical jet stream (Wen et al. 2009), the mid-high latitude circulation systems, such as the Siberian high and the polar vortex that bring cold anomalies to the eastern China (Gao 2009; Song and Wu 2017, 2018a). What are the factors and processes of intraseasonal variations of snow over the eastern China?

The present study addressed the following questions: 1) What is the dominant time scale of intraseasonal snow variation over the eastern China during boreal winter? 2) What are the factors and physical processes of intraseasonal snow variations over the eastern China? The rest of this study is organized as follows. Data and methodology are described in section 2. Main results are presented in section 3. A summary is provided in section 4.

2. Data and methodology

This study uses the latest satellite daily snow cover data from the MODIS/Terra Snow Cover Daily L3 Global 0.05Deg CMG, Version 6 (Hall and Riggs 2016). This data provide consistent and objective snow estimates through high-resolution visible light observation (Frei et al. 2012; Chen et al. 2016). The overall accuracy of the MODIS snow cover data is about 93% (Hall and Riggs 2007). This dataset is on the MODIS Climate Modeling Grid (CMG), which consists of 7200 columns by 3600

rows with a horizontal resolution of 0.05°×0.05°. The snow cover is represented by percentages of snow-covered land in 0.05° resolution CMG cells. The details for the above snow data can be found on the National Snow and Ice Data Center website (https://nsidc.org/data/modis/data_summaries#snow). We convert the original data on 0.05°×0.05° grid to 0.5°×0.5° grid. A 3-day running mean is further applied to 0.5°× 0.5° grid data to reduce the missing data. The snow cover data is only available south of 60°N during winter polar night. We focus on 15 winters (December-January-February) from 2004 to 2018.

The daily output from the National Centers for Environmental Prediction (NCEP)-Department of Energy (DOE) Reanalysis 2 provided by the NOAA/OAR/ESRL Physical Science Division (PSD) (Kanamitsu et al. 2002) is used in this study. The variables used include geopotential height, sea level pressure, meridional and zonal winds, vertical p-velocity, air temperature, surface air temperature and wind. The pressure level data at 17 layers from 1000 to 10-hPa have a horizontal resolution of 2.5°×2.5°. Surface data are available on the T62 Gaussian grid.

The daily North Atlantic Oscillation (NAO) index is obtained from the NOAA Climate Prediction Center (CPC) website (http://www.cpc.ncep.noaa.gov/products/precip/CWlink/pna/nao.shtml). The daily

Arctic Oscillation (AO) index is obtained from the NOAA (CPC) website (http://www.cpc.ncep.noaa.gov/products/precip/CWlink/daily_ao_index/ao.shtml). The intraseasonal variation is extracted using the Butterworth band-pass filter. Regression and composite analysis are employed to obtain anomalies of different quantities. The statistical significance level is estimated based on the Student's *t*-test. The propagation of tropospheric Rossby wave train is depicted by the Rossby wave activity fluxes (Takaya and Nakamura 2001).

3. Results

Snow cover over the eastern China displays obvious intraseasonal variations during boreal winter. Figure 1a presents the power spectrum of 15-year average area-mean (20-40°N, 105-120°E) snow cover during winter (December to February, DJF). Two spectrum peaks can be found at the time periods of 14 days and 8 days. Therefore, the dominant frequency of the intraseasonal snow cover variation over the eastern China is within 30 days.

The EOF analysis is applied to the 10-30-day intraseasonal snow cover variation in DJF over the eastern China (20-40°N, 105-120°E) that is extracted using the 10-30-day band-pass filter. The corresponding distribution of snow cover anomalies is displayed in Figure 1b that is the regression map with respect to the leading principal

time series (PC1). The leading mode accounts for 38.5% of the total variance, which is separated from the other modes based on the criterion of North et al. (1982). Two positive snow cover centers are observed, one over northwest part of the eastern China and the other located north of the Yangtze River. It is noted that the intraseasonal snow cover variations in the above regions are not linked to those over the Tibetan Plateau and Northeast China, in agreement with previous studies (Sun et al. 2010; Zhou et al. 2018).

Next, we perform a composite analysis based on the leading EOF mode to reveal the characteristics of 10-30-day snow cover variations over the eastern China. The normalized PC1 associated with the leading EOF is defined as an index for intraseasonal snow cover variation over the eastern China. If this index exceeds one positive standard deviation for three consecutive days, it is defined as an intraseasonal snow event, and the peak day is marked as day 0 of the snow event over the eastern China. We identified 25 snow events in the 15 winters from 2004 to 2018, which is listed in Table 1. Composite anomalies are obtained for these 25 snow events. All the variables have been filtered by a 10-30-day band-pass filter before composite analysis.

Snow cover anomalies manifest evident spatial-temporal evolution during intraseasonal snow events over the eastern China. On day -4 of snow events, negative

snow cover anomalies are located over the eastern China and southeast flank of the Tibetan Plateau (Figure 2a). The negative anomalies over the eastern China are weakened afterwards. On day -2, positive snow cover anomalies emerge over northwest part of the eastern China and north of the Yangtze River (Figure 2b). These positive snow cover anomalies reach the peak on day 0 (Figure 2c). After day 0, snow cover anomalies decrease (Figures 2d).

The variation of snow cover anomalies during snow events can be revealed by snow cover tendency. On day -4, positive snow cover tendency appears over northwest part of the eastern China and north of the Yangtze River (Figure 2e), which indicates snow cover accumulation. The positive snow cover tendency is enhanced on day -2 (Figure 2f), corresponding to the development of positive snow cover anomalies in situ (Figure 2b). The snow cover tendency becomes weak over the eastern China on day 0 (Figure 2g), suggesting the peak of snow cover anomalies (Figure 2c). The snow cover tendency turns to negative after day 0, indicating the weakening of positive snow cover anomalies (Figures 2d and 2h).

Snowfall over the eastern China needs both low temperature and high moisture (Sun and Wang 2013; Zhou et al. 2018). Here, we elaborate atmospheric circulation and surface temperature anomalies and water vapor transportation during snow events over the eastern China. Snow cover anomalies are accompanied by prominent surface

temperature anomalies. On day -4, evident cold anomalies appear over western Mongolia, and warm anomalies are located over southern coast of China (Figure 3a). The cold anomalies intrude the eastern China in the following days (Figure 3b), which are accompanied by positive snow cover tendency (Figure 2f). On day 0, the cold anomalies and snow cover anomalies over the eastern China reach the peak (Figures 3c and 2c) when the snow cover tendency is weak (Figure 2g). The cold anomalies are weakened over the eastern China on day 2 (Figure 3d), which correspond to the decrease of snow cover anomalies (Figures 2d and 2h). The temporal evolution of cold anomalies over the eastern China during snow events indicates a close relationship between the snowfall and low temperature anomalies.

The temperature anomalies are related to surface wind anomalies. On day -4, surface cyclonic anomalies are observed around the Lake Baikal, accompanied by surface southerly wind anomalies over northern China (Figure 3e). In the following days, the anticyclonic anomalies move southeastward with northerly wind anomalies dominating the eastern China (Figure 3f), which explain the southward intrusion of cold anomalies to the eastern China (Figure 3b). The anticyclonic anomalies continue to move southeastward on day 0 and diminish over the southeastern coast of China on day 2 (Figures 3g-3h), which is accompanied by the weakening of cold anomalies over the eastern China (Figure 3d).

The surface anticyclonic anomalies causing cold anomalies over the eastern China are associated with mid-latitude upper-tropospheric wave trains (Park et al. 2011; Song et al. 2016; Song and Wu 2017). On day -6, one branch of wave activity fluxes emits from cyclonic anomalies over the northern Scandinavia and moves along an anticyclonic-cyclonic-anticyclonic pattern over Eurasia towards the eastern China (Figure 4a). Another branch of wave activity fluxes emits from anticyclonic anomalies over the Mediterranean Sea and travels eastward along the subtropical jet (Hoskins and Ambrizzi 1993). The two braches merge on day -4 (Figure 4b) and contribute to the development of cyclonic anomalies over Central Asia and anticyclonic anomalies over East Asia. On day -2, the subtropical wave fluxes weaken over East Asia and another branch of wave activity fluxes appear over the Mediterranean Sea (Figure 4c). Meanwhile, the mid-latitude wave train moves eastward. On day 0, both the mid-latitude and subtropical wave activity fluxes contribute to the enhancement of cyclonic anomalies over East Asia (Figure 4d), which is followed by surface anticyclonic anomalies and the southward intrusion of cold air (Figures 3c and 3g) (Song and Wu 2017). It should be noted that the subtropical wave train is weaker than the mid-latitude wave train, which suggests a dominant role of the mid-high-latitude atmospheric circulation in the development of intraseasonal snow cover events over the eastern China.

The moisture for snowfall over the eastern China is related to the northward water vapor transportation. Northward transportation of water vapor appears over the southwestern flank of the anticyclonic anomalies over the eastern China on day -6 (Figures 4a and 4e). This leads to convergence of water vapor fluxes over southeastern China. On day -4, the above water vapor fluxes increase (Figure 4f). Correspondingly, water vapor convergence becomes larger. The water vapor fluxes turn westward over the eastern China and bring water vapor from the East China Sea, which leads to the positive snow cover tendency over the eastern China (Figure 2e). The easterly wind anomalies on the southern flank of the anticyclonic anomalies over East Asia (Figure 4b) contribute to the westward water vapor fluxes. Divergence of water vapor fluxes develops over the eastern China after day -4 (Figures 4g-h), which corresponds to the southward intrusion of surface anticyclonic anomalies (Figures 3f-3g) that bring cold and dry air from the high-latitudes (Figures 3b-3c). The northward water vapor fluxes are weakened on day -2 (Figure 4g). Divergence of water vapor fluxes dominates the southeast coast of China on day 0, which corresponds to surface anticyclonic anomalies and weakened snow cover tendency (Figures 3g and 2g).

The temporal evolutions of regional mean surface temperature and snow cover anomalies over the eastern China (20-40°N, 105-120°E) are further illustrated in

Figure 5a. Snow cover varies nearly out of phase with surface temperature during the snow events. Both the snow cover and surface temperature anomalies reach the peak on day 0,. This indicates that the cold anomalies provide condition for snow accumulation. The NAO index is positive on day -7 and -6. This suggests that the NAO triggers the subtropical wave train, consistent with previous study (Watanabe 2004). The AO index is negative from day -6 to day 1 and it reaches the peak on day -3, during which most part of the polar region is covered by anomalous anticyclone and cyclonic anomalies situate over the North Atlantic and North Pacific at lower level, corresponding to negative AO (figure not shown). The negative AO appears to contribute to the development of the mid-latitude Rossby wave train from day -6 to day 0 (Figures 4a-4d) (Park et al. 2011; Song and Wu 2018b). In comparison, the AO signal is much stronger than the NAO, and the subtropical wave train is not as evident as the mid-latitude wave train (Figures 4a-4d). Therefore, the development of snow events over the eastern China is mainly related to negative AO.

The temporal relationship between the snow cover variation and the atmospheric condition for snowfall are further demonstrated in Figure 5b. The snow cover tendency (calculated using central differentiation) turns to positive after day -7, indicating the snow accumulation over the eastern China (Figures 2a-2c and 2e-2g). The convergence of anomalous water vapor fluxes and anomalous ascending motion

at 700-hPa are evident after day -8. They reach the peak on day -4. The time-lag relationship indicates that snowfall is preceded by the accumulation of water vapor in the atmosphere. This validates that the water vapor transportation provides the moisture condition for snow events over the eastern China. The snow accumulation from day -4 to day -2 is accompanied by the decrease of anomalous water vapor flux convergence and the weakening of anomalous ascending motion. From day -2 to day 0, the snow continues to accumulate. At the same time, anomalous descending motion develops accompanying anomalous water vapor flux divergence. After day 0, snow melting begins, accompanying strong anomalous descending motion and water vapor divergence.

The snow cover tendency lags the moisture convergence and ascending motion. This is related to time lags between the moisture convergence and snowfall and between snowfall and snow accumulation on ground. The moisture convergence provides the moisture condition, and meanwhile, the ascending motion provides the dynamical condition for cloud/snow formation. The snowfall may lag the cloud formation by some time as it also depends upon the temperature condition. Whether the snow can accumulate on the ground when it falls also depends upon the surface temperature condition. As such, there is a time lag between the snow cover tendency and the moisture convergence and ascending motion.

4. Summary

By using the latest satellite daily snow cover date from the MODIS/Terra product, the present study documents the intraseasonal snow cover variations over the eastern China during boreal winter and the associated factors and the physical processes. It is found that the dominant time scale of intraseasonal snow cover variation over the eastern China is within 30 days. The present study focused on the 10-30-day intraseasonal variation extracted using a band-pass filter. The leading EOF mode of the 10-30-day snow cover variation over the eastern China has large loading over the northwest part of the eastern China and the north of the Yangtze River. Intraseasonal snow events over the eastern China are identified based on the normalized PC1. A composite analysis is conducted for 25 snow events identified in 15 winters (December to February) from 2004 to 2018.

The temporal evolution of composite anomalies reveals the following processes involved in intraseasonal snow cover variations over the eastern China. Negative AO contributes to the enhancement of a mid-latitude wave train, which is accompanied by a weak subtropical wave train. The two wave trains lead to the development and eastward move of cyclonic anomalies over Asia. This induces convergence of anomalous water vapor fluxes and anomalous ascending motion over the eastern

China, which provides the moisture condition for snowfall. Surface anticyclonic anomalies and accompanying surface northerly wind anomalies bring cold air toward the eastern China, which provides the temperature condition for snow accumulation. The snowfall leads to the switch of snow cover anomalies over the eastern China from negative anomalies to positive anomalies in about 2 days. Following the development of anomalous descending motion and water vapor divergence, snow starts to melt, leading to the decrease in snow cover.

Acknowledgments

We appreciate comments from two anonymous reviewers that have helped the improvement of this manuscript. This study is supported by the National Natural Science Foundation of China grants (41705063, 41530425, 41721004, 41775080 and 41475081). The NCEP reanalysis 2 data were obtained from ftp://ftp.cdc.noaa.gov/. The snow cover data were obtained from the National Snow and Ice Data Center (https://nsidc.org/data/modis/data_summaries#snow).

References

Chen, X., S. Liang, Y. Cao, and T. He (2016), Distribution, attribution, and radiative forcing of snow cover changes over China from 1982 to 2013, *Climatic Change*, 137(3), 363-377, doi:10.1007/s10584-016-1688-z.

Frei, A., M. Tedesco, S. Lee, J. Foster, D. K. Hall, R. Kelly, and D. A. Robinson (2012), A review of global satellite-derived snow products, *Advances in Space Research*, 50(8), 1007-1029, doi:https://doi.org/10.1016/j.asr.2011.12.021.

Hall, D. K., and G. A. Riggs (2007), Accuracy assessment of the MODIS snow products, *Hydrological Processes*, 21(12), 1534-1547, doi:10.1002/hyp.6715.

Hall, D. K. a. G. A. R. (2016), MODIS/Terra Snow Cover Daily L3 Global 0.05Deg CMG, Version 6, Boulder, Colorado USA. NASA National Snow and Ice Data Center Distributed Active Archive Center, doi:https://doi.org/10.5067/MODIS/MOD10C1.006.

Hoskins, B. J., and T. Ambrizzi (1993), Rossby wave propagation on a realistic longitudinally varying flow, *Journal of the Atmospheric Sciences*, 50(12), 1661-1671, doi:10.1175/1520-0469(1993)050<1661:RWPOAR>2.0.CO;2.

Hui, G. (2009), China's snow disaster in 2008, who is the principal player?, *International Journal of Climatology*, 29(14), 2191-2196, doi:10.1002/joc.1859.

Kanamitsu, M., W. Ebisuzaki, J. Woollen, S.-K. Yang, J. J. Hnilo, M. Fiorino, and G. L. Potter (2002), NCEP–DOE AMIP-II Reanalysis (R-2), *Bulletin of the American Meteorological Society*, 83(11), 1631-1643, doi:10.1175/BAMS-83-11-1631.

Li, X., Y. D. Chen, and W. Zhou (2017), Response of winter moisture circulation to the India–Burma trough and its modulation by the South Asian waveguide, *Journal of Climate*, 30(4), 1197-1210, doi:10.1175/jcli-d-16-0111.1.

North, G. R., T. L. Bell, R. F. Cahalan, and F. J. Moeng (1982), Sampling errors in the estimation of empirical orthogonal functions, *Monthly Weather Review*, 110(7), 699-706, doi:10.1175/1520-0493(1982)110<0699:seiteo>2.0.co;2.

Park, T.-W., C.-H. Ho, and S. Yang (2011), Relationship between the Arctic Oscillation and cold surges over East Asia, *Journal of Climate*, 24(1), 68-83, doi:10.1175/2010JCLI3529.1.

Song, L., L. Wang, W. Chen, and Y. Zhang (2016), Intraseasonal variation of the strength of the East Asian trough and its climatic impacts in boreal winter, *Journal of Climate*, doi:10.1175/JCLI-D-14-00834.1.

Song, L., and R. Wu (2017), Processes for occurrence of strong cold events over eastern China, *Journal of Climate*, 30(22), 9247-9266, doi:10.1175/jcli-d-16-0857.1.

Song, L., and R. Wu (2018a), Precursory signals of East Asian winter cold anomalies in stratospheric planetary wave pattern, *Climate Dynamics*, doi:10.1007/s00382-018-4491-x.

Song, L., and R. Wu (2018b), Comparison of intraseasonal East Asian winter cold temperature anomalies in positive and negative phases of the Arctic Oscillation, *Journal of Geophysical Research: Atmospheres*, 123(16), 8518-8537, doi:10.1029/2018JD028343.

Sun, B., and H. Wang (2013), Water vapor transport paths and accumulation during widespread snowfall events in northeastern China, *Journal of Climate*, 26(13), 4550-4566, doi:10.1175/jcli-d-12-00300.1.

Sun, J., H. Wang, W. Yuan, and H. Chen (2010), Spatial-temporal features of intense snowfall events in China and their possible change, *Journal of Geophysical Research: Atmospheres*, 115(D16), doi:doi:10.1029/2009JD013541.

Takaya, K., and H. Nakamura (2001), A formulation of a phase-independent wave-activity flux for stationary and migratory quasigeostrophic eddies on a zonally varying basic flow, *Journal of the Atmospheric Sciences*, 58(6), 608-627, doi:10.1175/1520-0469(2001)058<0608:afoapi>2.0.co;2.

Watanabe, M. (2004), Asian jet waveguide and a downstream extension of the North Atlantic Oscillation, *Journal of Climate*, 17(24), 4674-4691, doi:10.1175/JCLI-3228.1.

Wen, M., S. Yang, A. Kumar, and P. Zhang (2009), An Analysis of the large-scale climate anomalies associated with the snowstorms affecting China in January 2008, *Monthly Weather Review*, 137(3), 1111-1131, doi:10.1175/2008mwr2638.1.

Zhou, B., et al. (2011), The great 2008 Chinese ice storm: Its socioeconomic–ecological impact and sustainability lessons learned, *Bulletin of the American Meteorological Society*, 92(1), 47-60, doi:10.1175/2010bams2857.1.

Zhou, B., Z. Wang, and Y. Shi (2017), Possible role of Hadley circulation strengthening in interdecadal intensification of snowfalls over northeastern China under climate change, *Journal of Geophysical Research: Atmospheres*, 122(21), 11,638-611,650, doi:10.1002/2017JD027574.

Zhou, B., Z. Wang, Y. Shi, Y. Xu, and Z. Han (2018), Historical and future changes of snowfall events in China under a warming background, *Journal of Climate*, 31(15), 5873-5889, doi:10.1175/jcli-d-17-0428.1.

Zhou, W., J. C. L. Chan, W. Chen, J. Ling, J. G. Pinto, and Y. Shao (2009), Synoptic-scale controls of persistent low temperature and icy weather over southern

China in January 2008, *Monthly Weather Review*, 137(11), 3978-3991, doi:10.1175/2009mwr2952.1.

Figure captions

Figure 1 (a) Power spectrum of the 15-year average area-mean snow cover over the region of 20-40°N, 105-120°E during December to February. Upper and lower curves indicate the 95% and 5% confidence level bounds, respectively. Middle curve denotes theoretical Markov spectrum. (b) Snow cover anomalies (%) obtained by regression onto normalized PC1 of 10-30-day band-pass filtered snow cover over the region of 20-40°N, 105-120°E during 15 winters from 2004 to 2018. Black dots denote snow cover anomalies significant at the 95% confidence level.

Figure 2 Composite snow cover anomalies (%) on day -4 (a), day -2 (b), day 0 (c), day 2 (d), and snow cover tendency (%/day) on day -4 (e), day -2 (f), day 0 (g), day 2 (h) of snow events. The black dots denote anomalies significant at the 95% confidence level.

Figure 3 Composite surface air temperature anomalies (shading, °C, scale in the upper bar) on day -4 (a), day -2 (b), day 0 (c), day 2 (d) of snow events. The black dots denote temperature anomalies significant at the 95% confidence level. Composite surface wind anomalies (vector, scale at right bottom of subplot (d)) and sea level pressure anomalies (shading, hPa, scale in the lower bar) on day -4 (e), day -2 (f), day 0 (g), day 2 (h) of snow events. Black vectors denote wind anomalies significant at the 95% confidence level.

Figure 4 Composite geopotential height anomalies at 300-hPa (shading, gpm, scale in the upper bar) and wave activity fluxes (vector, scale at right bottom of subplot (d)) on day -6 (a), day -4 (b), day -2(c), day 0 (d) of snow events. Composite water vapor flux integral from 1000 to 100-hPa (vector, scale at right bottom of subplot (h)) and its divergence (shading, $*10^{-5}$ kg/m^2*s, scale in the lower bar) on day -6 (e), day -4 (f), day -2 (g), day 0 (h) of snow events.

Figure 5 (a) Time evolution of composite NAO index (pink curve), AO index (blue curve), regional mean surface air temperature anomalies (°C) (black curve) and snow cover anomalies (%) (red curve) in the region of 20-40°N, 105-120°E. (b) Time evolution of composite anomalies of regional mean snow cover tendency (%/day) (black curve), vertical velocity (Pa/s) (blue curve), and divergence of water vapor flux integral from 1000 to 100-hPa ($*10^{-6}$ kg/(m^2*s)) (pink curve) in the region of 20-40°N, 105-120°E. Dots on the curves indicate anomalies significant at the 95% confidence level.

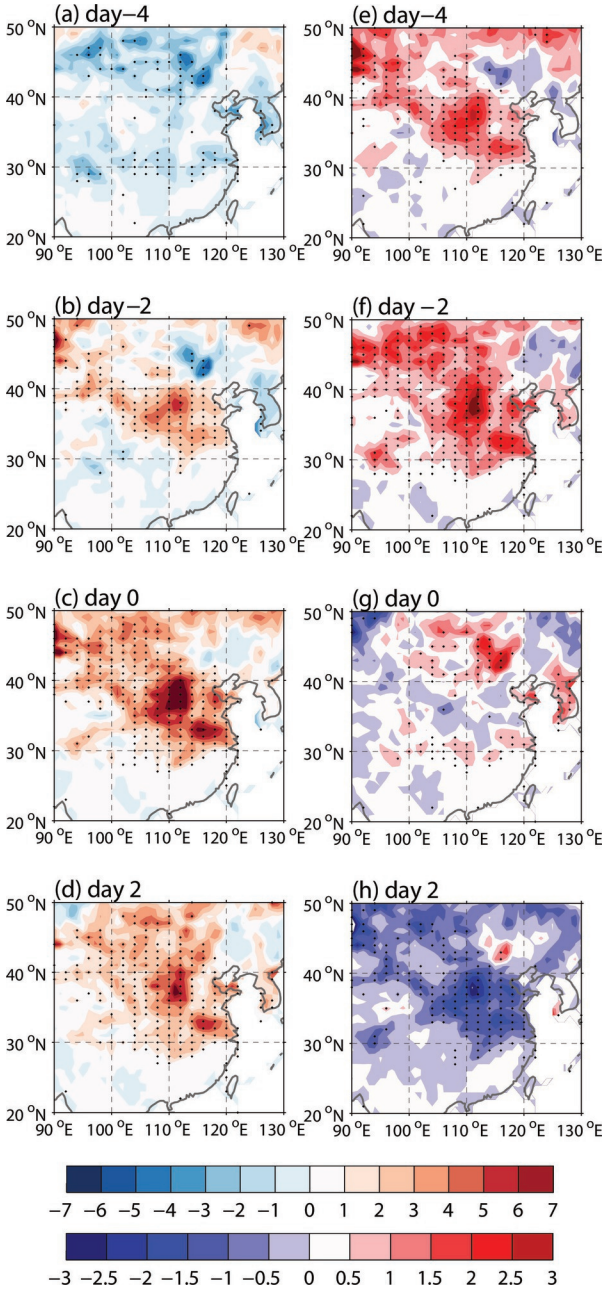

asl2_901_fig_2.eps

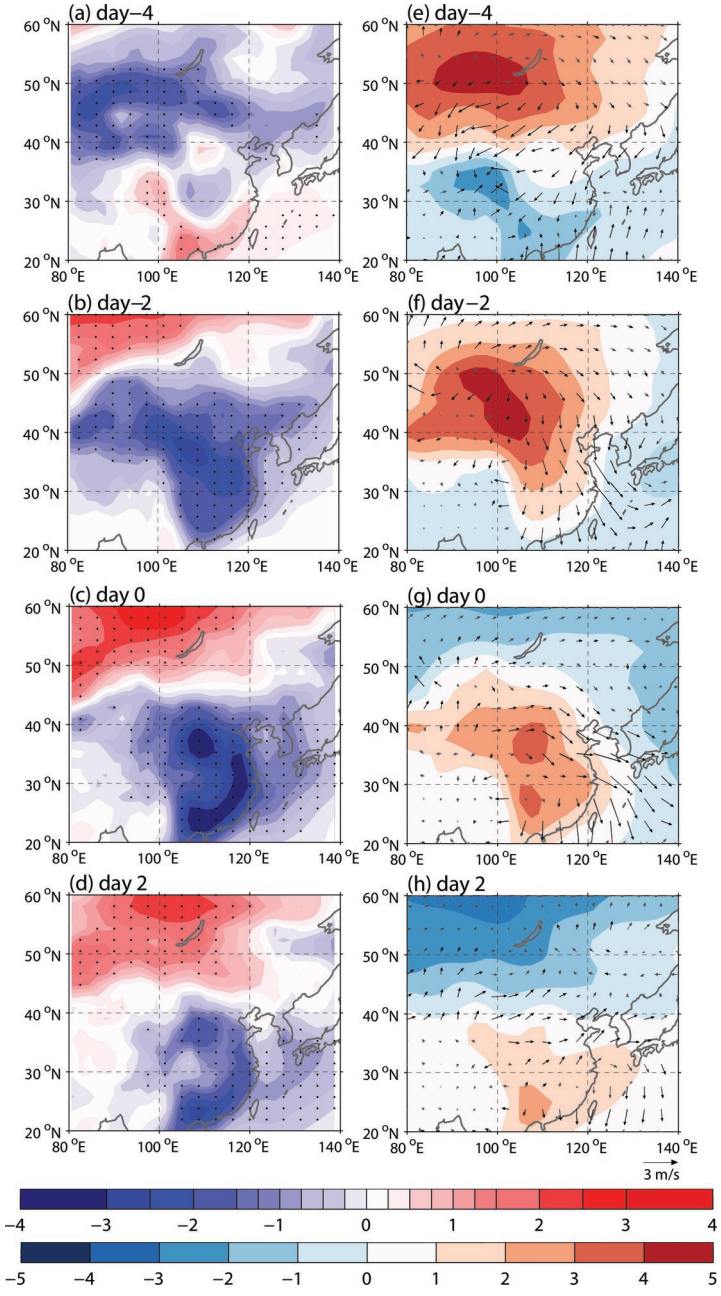

asl2_901_fig_3.eps

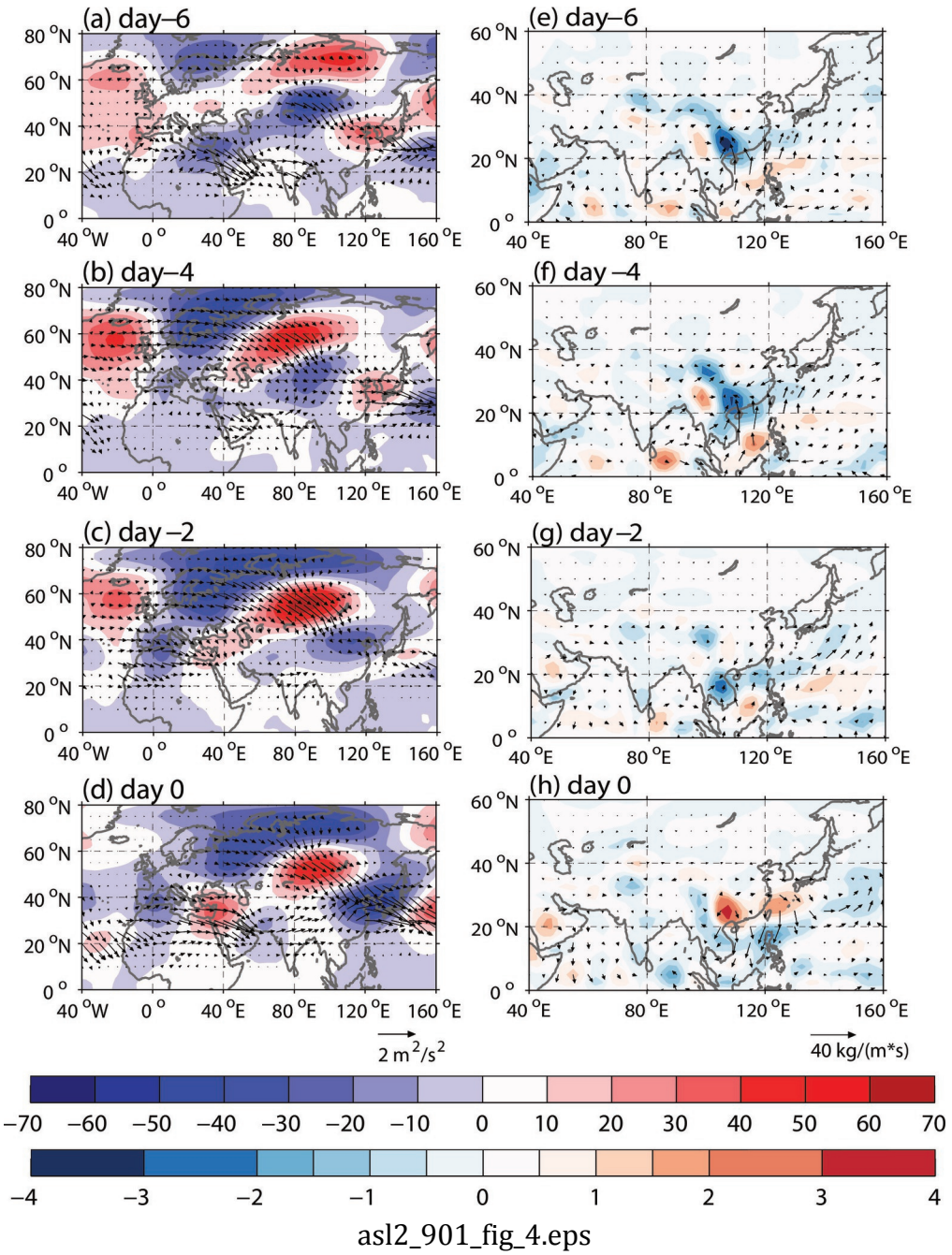

asl2_901_fig_4.eps

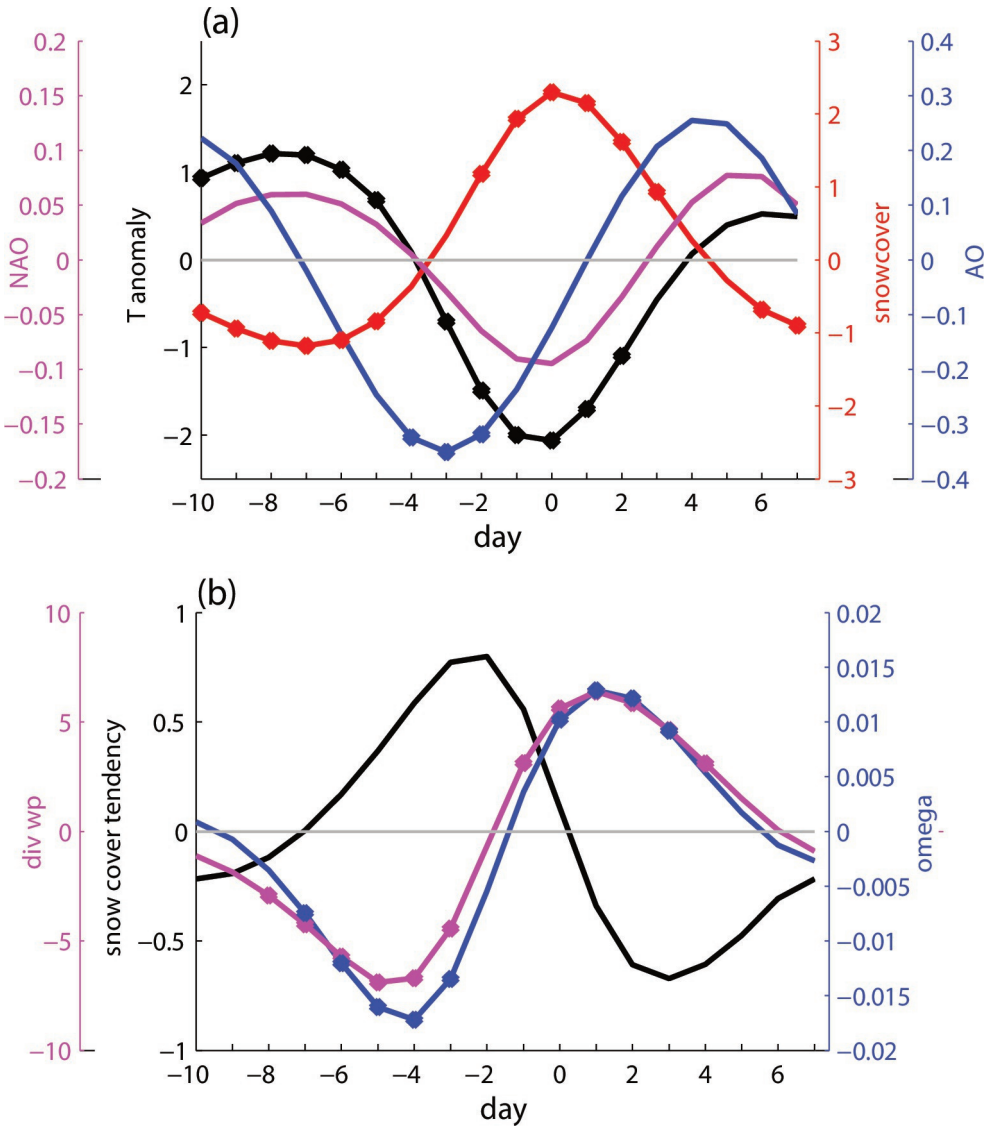

asl2_901_fig_5.eps

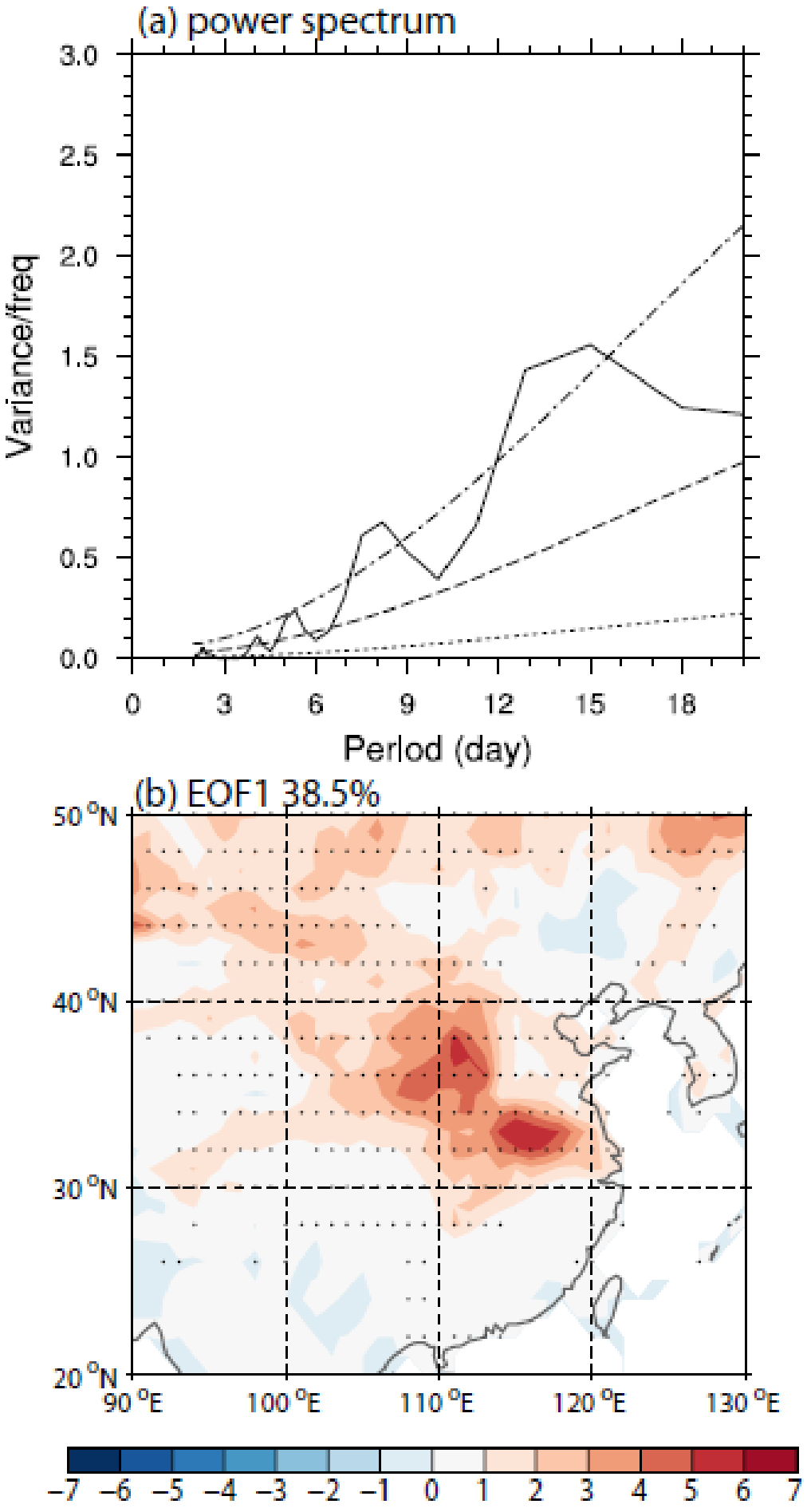

ASL2_901_Figure 1.PNG

Table 1 The year and day 0 of snow events.

Year	Snow events	Year	Snow events
2003-2004	Dec 12; Jan 19	2011-2012	Dec 10; Jan 25
2004-2005	Jan 2; Feb 20	2012-2013	Dec 24; Jan 24;
2005-2006	Jan 7; Jan 23; Feb 8	2013-2014	Feb 10; Feb 20
2006-2007	Feb 9	2015-2016	Dec 16; Jan 24; Feb 15
2007-2008	Feb 3	2016-2017	Dec 29; Feb 23
2009-2010	Dec 19; Feb 13	2017-2018	Jan 9; Jan 30
2010-2011	Feb 14		